Transcendental Mode Shape Development for Vibration Analysis of a Pinned–Pinned Double-Overhung Beam with End Lumped Masses

Bishal Kumar [1, 2,*], Mahesh Chandra Luintel[1], Debendra Bahadur Raut[2], Surya Prasad Adhikari[1]

[1]Department of Mechanical and Aerospace Engineering, Pulchowk Campus, Institute of Engineering, Tribhuvan University, Pulchowk, Lalitpur, Nepal

[2]Department of Automobile and Mechanical Engineering, Thapathali Campus, Institute of Engineering, Tribhuvan University, Thapathali, Kathmandu, Nepal

*jhabishal12@gmail.com

(Manuscript Received: 28th January, 2026; Revised: 10th February, 2026; Accepted: 17th February, 2026)

Abstract

This study presents a transcendental mode shape formulation for the vibration analysis of a pinned–pinned double-overhung beam carrying lumped masses at both free overhung ends. The beam is modeled as a slender Euler–Bernoulli beam, with shear deformation and rotary inertia neglected. The governing differential equation for free transverse vibration is solved analytically by enforcing boundary conditions at the pinned supports and continuity and equilibrium conditions at the locations of the lumped masses. This procedure yields transcendental frequency equations and the corresponding mode shape functions. The first three bending natural frequencies obtained from the analytical solution are 4.9396 Hz, 7.016 Hz, and 71.9266 Hz, respectively. To validate the analytical formulation, numerical simulations are carried out using a finite element–based model. The corresponding natural frequencies from the numerical analysis are 7.4583 Hz, 7.0189 Hz, and 81.537 Hz. The proposed analytical formulation provides an effective framework for the vibration analysis of double-overhung beams with lumped masses and can serve as a reliable reference for further analytical and numerical investigations in beam dynamics.

Keywords: Pinned-pinned, Double overhung, transverse vibration, Euler-Bernoulli beam, lumped mass, Transcendental

1. Introduction

Machine tool spindles, crane arms, robotic manipulators, bridge decks, and rotating shafts with attached components are just a few of the engineering applications that frequently use beams with overhangs and related discrete masses. Functional needs like tool holders, payloads, sensors, joints, or supplementary mechanical attachments give birth to overhanging segments and concentrated masses in these systems.

By changing the stiffness distribution, mass participation, and boundary conditions, these discrete features have a substantial impact on the structure's dynamic properties. Because of this, precise modelling of overhung beams with lumped masses is necessary for safe and effective engineering system design, resonance avoidance, and accurate vibration behaviour prediction.

By introducing geometric discontinuities and local inertia effects, overhangs and lumped masses dramatically modify the dynamic properties of beam-like structures. This can result in major variations in natural frequencies and mode shapes. For dependable design, vibration control, and structural integrity evaluation, accurate prediction of these dynamic features is crucial.

Pinned-pinned beams with double overhangs are a significant structural type in real-world engineering systems among several support configurations. The interaction between the concentrated inertial effects of the connected masses and the scattered mass of the beam causes the dynamic behaviour to become more complex when lumped masses are added at the free ends of the overhangs. When discrete masses and overhung segments are added, the well-established classical methods for

homogeneous beams without overhangs or attached masses are no longer immediately relevant.

In vibration analysis, it is crucial to accurately characterize the interplay between continuous beam structures and discrete attachments. This interaction was investigated for beams carrying spring–mass systems using the dynamic stiffness technique, showing how discrete masses and elastic supports may be incorporated analytically while capturing their coupled modal behaviour (Banerjee, 2012).

By examining beams with several masses and springs, another study expanded on these ideas. Their experimental and analytical findings demonstrated that the natural frequencies and mode shapes are strongly influenced by the attached masses' position and size. The significance of explicitly incorporating discrete parts in beam vibration modelling was emphasized by this work, particularly for complex systems with numerous attachments (Wang et al., 2014).

A new study helped further obtain accurate closed-form solutions for the bending vibrations of wedge beams carrying any number of point masses in the setting of beams with multiple point masses. By dividing the beam into segments and enforcing displacement continuity and force balancing at each mass position using Euler-Bernoulli beam theory, they were able to provide precise formulas for the natural frequencies and mode shapes of non-uniform beams with numerous concentrated masses (Wu & Chen, 2003).

Another new work demonstrated precise estimation of natural frequencies and mode shapes for beams with attached masses by using the harmonic differential quadrature (HDQ) approach to analyze free vibration of elastic beams. Their study bridged the gap between purely numerical and closed-form analytical methods by validating the usefulness of semi-analytical techniques in modelling beams with both continuous and discrete constituents (Civalek & Ülker, 2004).

Further, a new study presented an analytical study of a simply supported beam with an overhang supporting a point mass at the free end. This arrangement was relevant to machine tool spindles and boring bars. They developed closed-form formulations for natural frequencies and mode shapes using Euler-Bernoulli beam theory by applying boundary and continuity requirements at the overhang. The results showed good agreement when evaluated using finite element analysis. The study demonstrated that the analytical solution could efficiently predict dynamic behaviour and optimize mass and support placement without the need for time-consuming numerical simulations, making it a valuable tool for vibration analysis and the design of overhung beam-mass systems (Alzghoul et al., 2022).

The explicit analytical derivation of transcendental mode shape functions for pinned–pinned double-overhung beams carrying lumped masses at both free overhung ends has received little attention despite these developments. Simpler arrangements, including beams with a single overhang or beams with a single or intermediate concentrated mass, have been the main focus of previous research. As a result, nothing is known about how end-attached lumped masses and double overhangs interact to affect the modal properties.

A thorough transcendental mode shape formulation for the free vibration analysis of a pinned–pinned double-overhung beam with lumped masses attached at both overhung ends is developed in this paper to fill this gap. The necessary transcendental frequency equations are methodically established, and correct analytical formulations for the mode shape functions are obtained using Euler–Bernoulli beam theory. These equations capture the combined effects of multiple inertia discontinuities and double overhang geometry, which greatly increase the analytical complexity when compared to conventional beam systems.

The suggested formulation provides a strong analytical foundation for comprehending the dynamic behaviour of intricate beam-mass systems pertinent to real-world engineering applications by enabling precise prediction of natural frequencies and mode shapes.

2. Free vibration analysis

Fig. 1 below shows a pinned-pinned double overhung beam with a lumped mass at either of the free overhung ends. The beam used here is assumed to be uniform, slender, and is subjected to transverse vibration, which is explicitly bending vibration in the xy plane.

Since the scope of the present study is confined to the free vibration analysis of a uniform beam, the governing differential equation is formulated using the classical Euler–Bernoulli beam theory, as expressed in (Rao, 2017).

In this formulation, the effects of shear deformation and rotary inertia are neglected, which is a valid assumption for slender beams where the length-to-thickness ratio is sufficiently large. This simplification allows for an analytical treatment of the vibration characteristics while maintaining reasonable accuracy for the types of beams considered in this study.

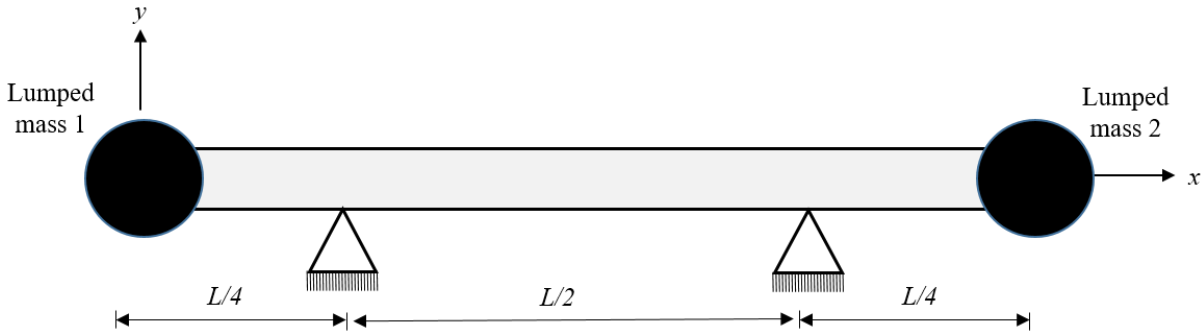

Fig. 1: Pinned-pinned double overhung beam

$$EI\frac{\partial^4 w}{\partial x^4}(x,t) + \rho A\frac{\partial^2 w}{\partial t^2}(x,t) = 0 \tag{1}$$

Where E is the Elastic Modulus for the beam material, I signifies the moment of inertia of the beam cross-section, w is the vertical displacement, t is time, ρ is the density of the beam, and A is the area of cross-section for the beam.

The solution of **Equation (1)** is obtained using the method of separation of variables. Using the method of separation of variables as shown in (Luintel, 2023), the solution of **Equation (1)** takes the form,

$$w(x,t) = Y(x)T(t) \tag{2}$$

The solution of the spatial domain of **Equation (2)** can be written explicitly in piecewise form for the problem formulation shown in **Fig. 1** as,

$$Y(x) = \begin{cases} Y_1(x), & 0 \le x \le \dfrac{L}{4} \\ Y_2(x), & \dfrac{L}{4} \le x \le \dfrac{3L}{4} \\ Y_3(x), & \dfrac{3L}{4} \le x \le L \end{cases} \tag{3}$$

$Y_1(x)$, $Y_2(x,)$ and $Y_3(x)$ can be expressed in transcendental equation form as,

$$Y_1(x) = A\,sin(\beta x) + B\cos(\beta x) + C\,sinh(\beta x) + D\,cosh(\beta x) \tag{4}$$

$$Y_2(x) = E\,sin(\beta x) + F\cos(\beta x) + G\,sinh(\beta x) + H\,cosh(\beta x) \tag{5}$$

$$Y_3(x) = I\,sin(\beta x) + J\cos(\beta x) + K\,sinh(\beta x) + M\,cosh(\beta x) \tag{6}$$

In **Equation (4)**, **Equation (5)**, and **Equation (6),** β represents the eigenvalue in the beam's transverse bending vibration in the xy plane.

2.1 Boundary condition implication and development of non-trivial state

For the case presented in **Fig. 1**, the boundary conditions from the left-most section to right most section are established at the left free end, first pin, second pin, and the right free end, respectively.

At the left overhung or the point of application of the first lump mass, the moment is zero, and a jump in shear force value is observed.

$$\frac{d^2Y_1(0)}{dx^2} = 0 \tag{7}$$

$$\frac{d^3Y_1(0)}{dx^3} - \frac{m_1\beta^4}{\rho A}Y_1(0) = 0 \tag{8}$$

At the first pin or left pin, deflection is zero, and there exists continuity in deflection, slope, and moment, respectively.

$$Y_1\left(\frac{L}{4}\right) = 0 \tag{9}$$

$$\frac{dY_1\left(\frac{L}{4}\right)}{dx} - \frac{dY_2\left(\frac{L}{4}\right)}{dx} = 0 \tag{10}$$

$$Y_2\left(\frac{L}{4}\right) = 0 = 0 \tag{11}$$

$$\frac{d^2Y_1\left(\frac{L}{4}\right)}{dx^2} - \frac{d^2Y_2\left(\frac{L}{4}\right)}{dx^2} = 0 \tag{12}$$

At the second pin or right pin, deflection is zero, and there exists continuity in deflection, slope, and moment, respectively.

$$Y_2\left(\frac{3L}{4}\right) = 0 \tag{13}$$

$$Y_3\left(\frac{3L}{4}\right) = 0 \tag{14}$$

$$\frac{dY_2\left(\frac{3L}{4}\right)}{dx} - \frac{dY_3\left(\frac{3L}{4}\right)}{dx} = 0 \tag{15}$$

$$\frac{d^2Y_2\left(\frac{3L}{4}\right)}{dx^2} - \frac{d^2Y_3\left(\frac{3L}{4}\right)}{dx^2} = 0 \tag{16}$$

At the right overhung or the point of application of the second lump mass, the moment is zero, and a jump in shear force value is observed.

$$\frac{d^2Y_3(L)}{dx^2} = 0 \tag{17}$$

$$\frac{d^3Y_3(L)}{dx^3} - \frac{m_2\beta^4}{\rho A}Y_3(L) = 0 \tag{18}$$

The boundary conditions on back-substitution in **Equation (4)**, **Equation (5),** and **Equation (6)** lead to the development of new forms of equations as shown below.

$$B - D = 0 \tag{19}$$

$$A + B\frac{m_1\beta}{\rho A} - C + D\frac{m_1\beta}{\rho A} = 0 \tag{20}$$

$$A\sin\left(\frac{\beta L}{4}\right) + B\cos\left(\frac{\beta L}{4}\right) + C\sinh\left(\frac{\beta L}{4}\right) + D\cosh\left(\frac{\beta L}{4}\right) = 0 \tag{21}$$

$$A\cos\left(\frac{\beta L}{4}\right) - B\sin\left(\frac{\beta L}{4}\right) + C\cosh\left(\frac{\beta L}{4}\right) + D\sinh\left(\frac{\beta L}{4}\right) - E\cos\left(\frac{\beta L}{4}\right) + F\sin\left(\frac{\beta L}{4}\right) - G\cosh\left(\frac{\beta L}{4}\right) - H\sinh\left(\frac{\beta L}{4}\right) = 0 \quad (22)$$

$$E\sin\left(\frac{\beta L}{4}\right) + F\cos\left(\frac{\beta L}{4}\right) + G\sinh\left(\frac{\beta L}{4}\right) + H\cosh\left(\frac{\beta L}{4}\right) = 0 \quad (23)$$

$$-A\sin\left(\frac{\beta L}{4}\right) - B\cos\left(\frac{\beta L}{4}\right) + C\sinh\left(\frac{\beta L}{4}\right) + D\cosh\left(\frac{\beta L}{4}\right) + E\sin\left(\frac{\beta L}{4}\right) + F\cos\left(\frac{\beta L}{4}\right) - G\sinh\left(\frac{\beta L}{4}\right) - H\cosh\left(\frac{\beta L}{4}\right) = 0 \quad (24)$$

$$E\sin\left(\frac{3\beta L}{4}\right) + F\cos\left(\frac{3\beta L}{4}\right) + G\sinh\left(\frac{3\beta L}{4}\right) + H\cosh\left(\frac{3\beta L}{4}\right) = 0 \quad (25)$$

$$I\sin\left(\frac{3\beta L}{4}\right) + J\cos\left(\frac{3\beta L}{4}\right) + K\sinh\left(\frac{3\beta L}{4}\right) + M\cosh\left(\frac{3\beta L}{4}\right) = 0 \quad (26)$$

$$E\cos\left(\frac{3\beta L}{4}\right) - F\sin\left(\frac{3\beta L}{4}\right) + G\cosh\left(\frac{3\beta L}{4}\right) + H\sinh\left(\frac{3\beta L}{4}\right) - I\cos\left(\frac{3\beta L}{4}\right) + J\sin\left(\frac{3\beta L}{4}\right) - K\cosh\left(\frac{3\beta L}{4}\right) - M\sinh\left(\frac{3\beta L}{4}\right) = 0 \quad (27)$$

$$-E\sin\left(\frac{3\beta L}{4}\right) - F\cos\left(\frac{3\beta L}{4}\right) + G\sinh\left(\frac{3\beta L}{4}\right) + H\cosh\left(\frac{3\beta L}{4}\right) + I\sin\left(\frac{3\beta L}{4}\right) + J\cos\left(\frac{3\beta L}{4}\right) - K\sinh\left(\frac{3\beta L}{4}\right) - M\cosh\left(\frac{3\beta L}{4}\right) = 0 \quad (28)$$

$$-I\sin(\beta L) - J\cos(\beta L) + K\sinh(\beta L) + M\cosh(\beta L) = 0 \quad (29)$$

$$I\left[-\cos(\beta L) + \frac{m_2\beta}{\rho A}\sin(\beta L)\right] + J\left[\sin(\beta L) + \frac{m_2\beta}{\rho A}\cos(\beta L)\right] + K\left[\cosh(\beta L) + \frac{m_2\beta}{\rho A}\sinh(\beta L)\right] + M\left[\sinh(\beta L) + \frac{m_2\beta}{\rho A}\cosh(\beta L)\right] = 0 \quad (30)$$

The above mentioned forms of transcendental equations from **Equation (19)** to **Equation (30**) lead to the evolution of a new set of equations which shows non trivial solution.

Encompassing all coefficients A, B, C, D, E, F, G, H, I, J, K, and M at an instant in a 12 by 12 matrix is tedious; this problem can be addressed using the idea of matrix partitioning.

$$\text{Coefficient matrix} = \begin{bmatrix} C_1 & C_2 \\ C_3 & C_4 \end{bmatrix} \quad (31)$$

Where,

$$C_1 = \begin{bmatrix} 0 & 1 & 0 & -1 & 0 & 0 \\ 1 & \frac{m_1\beta}{\rho A} & -1 & \frac{m_1\beta}{\rho A} & 0 & 0 \\ \sin\left(\frac{\beta L}{4}\right) & \cos\left(\frac{\beta L}{4}\right) & \sinh\left(\frac{\beta L}{4}\right) & \cosh\left(\frac{\beta L}{4}\right) & 0 & 0 \\ \cos\left(\frac{\beta L}{4}\right) & -\sin\left(\frac{\beta L}{4}\right) & \cosh\left(\frac{\beta L}{4}\right) & \sinh\left(\frac{\beta L}{4}\right) & -\cos\left(\frac{\beta L}{4}\right) & \sin\left(\frac{\beta L}{4}\right) \\ 0 & 0 & 0 & 0 & \sin\left(\frac{\beta L}{4}\right) & \cos\left(\frac{\beta L}{4}\right) \\ -\sin\left(\frac{\beta L}{4}\right) & -\cos\left(\frac{\beta L}{4}\right) & \sinh\left(\frac{\beta L}{4}\right) & \cosh\left(\frac{\beta L}{4}\right) & \sin\left(\frac{\beta L}{4}\right) & \cos\left(\frac{\beta L}{4}\right) \end{bmatrix}$$

$$C_2 = \begin{bmatrix} 0 & 0 & 0 & 0 & 0 & 0 \\ 0 & 0 & 0 & 0 & 0 & 0 \\ 0 & 0 & 0 & 0 & 0 & 0 \\ -\cosh\left(\frac{\beta L}{4}\right) & -\sinh\left(\frac{\beta L}{4}\right) & 0 & 0 & 0 & 0 \\ \sinh\left(\frac{\beta L}{4}\right) & \cosh\left(\frac{\beta L}{4}\right) & 0 & 0 & 0 & 0 \\ -\sinh\left(\frac{\beta L}{4}\right) & -\cosh\left(\frac{\beta L}{4}\right) & 0 & 0 & 0 & 0 \end{bmatrix}$$

$$C_3 = \begin{bmatrix} 0 & 0 & 0 & 0 & \sin\left(\frac{3\beta L}{4}\right) & \cos\left(\frac{3\beta L}{4}\right) \\ 0 & 0 & 0 & 0 & 0 & 0 \\ 0 & 0 & 0 & 0 & \cos\left(\frac{3\beta L}{4}\right) & -\sin\left(\frac{3\beta L}{4}\right) \\ 0 & 0 & 0 & 0 & -\sin\left(\frac{3\beta L}{4}\right) & -\cos\left(\frac{3\beta L}{4}\right) \\ 0 & 0 & 0 & 0 & 0 & 0 \\ 0 & 0 & 0 & 0 & 0 & 0 \end{bmatrix}$$

$$C_4 = \begin{bmatrix} \sinh\left(\frac{3\beta L}{4}\right) & \cosh\left(\frac{\beta L}{4}\right) & 0 & 0 & 0 & 0 \\ 0 & 0 & \sin\left(\frac{3\beta L}{4}\right) & \cos\left(\frac{3\beta L}{4}\right) & \sinh\left(\frac{3\beta L}{4}\right) & \cosh\left(\frac{\beta L}{4}\right) \\ \cosh\left(\frac{\beta L}{4}\right) & \sinh\left(\frac{3\beta L}{4}\right) & -\cos\left(\frac{3\beta L}{4}\right) & \sin\left(\frac{3\beta L}{4}\right) & -\cosh\left(\frac{\beta L}{4}\right) & -\sinh\left(\frac{3\beta L}{4}\right) \\ \sinh\left(\frac{3\beta L}{4}\right) & \cosh\left(\frac{\beta L}{4}\right) & \sin\left(\frac{3\beta L}{4}\right) & \cos\left(\frac{3\beta L}{4}\right) & -\sinh\left(\frac{3\beta L}{4}\right) & -\cosh\left(\frac{\beta L}{4}\right) \\ 0 & 0 & -\sin(\beta L) & -\cos(\beta L) & \sinh(\beta L) & \cosh(\beta L) \\ 0 & 0 & -\cos(\beta L) + \frac{m_2\beta}{\rho A}\sin(\beta L) & \sin(\beta L) + \frac{m_2\beta}{\rho A}\cos(\beta L) & \cosh(\beta L) + \frac{m_2\beta}{\rho A}\sinh(\beta L) & \sinh(\beta L) + \frac{m_2\beta}{\rho A}\cosh(\beta L) \end{bmatrix}$$

Solving the 12 by 12 matrix obtained above, the value of βL can be evaluated for the parameter values as shown in **Table 1**.

Table 1: Value of parameters of the beam

Parameters	**Values**
Length of beam (L)	1 m
Density of beam material (ρ)	7850 kg/m^3
Young's Modulus of beam material (E)	200 GPa
Lumped Mass 1	0.500 kg
Lumped Mass 2	0.500 kg
Area of beam cross-section (A)	25 mm^2
Moment of Inertia (I)	52.083 mm^4

The value of βL for the first three bending modes is found to be 2.064, 2.460, and 7.876, respectively, and the natural frequency corresponding to the value of βL can be obtained from the relation,

$$f_n = \frac{{\beta_n}^2}{2\pi}\sqrt{\frac{EI}{\rho A}}$$

The natural frequencies corresponding to the first three transverse bending vibration modes are found to be 4.9396 Hz, 7.016 Hz, and 71.9266 Hz, respectively.

2.2 Transcendental mode shape

The coefficients A, B, C, D, E, F, G, H, I, J, K, and M must be evaluated to deduce the mode shapes. Nevertheless, the equations available are not sufficient to calculate the coefficients. Therefore, coefficients need to be normalized by dividing by A coefficient to determine the value of each coefficient A, B, C, D, E, F, G, H, I, J, K, and M.

When the value of βL obtained is substituted in sets of equations from **Equation (19)** to **Equation (30)**, the value of normalized coefficients is evaluated, which leads to the development of a transcendental piecewise mode shapes equation as,

$$Y(x)_{First\ mode} = \begin{cases} \sin(2.064358612x) - 0.1344972062\cos(2.064358612x) \\ -0.4147794446sinh(2.064358612x) - 0.1344972062cosh(2.064358612x), & 0 \le x \le \frac{L}{4} \\ 0.3715957259\sin(2.064358612x) + 0.2220475262\cos(2.064358612x) \\ +0.4061013764sinh(2.064358612x) - 0.5241499288cosh(2.064358612x), & \frac{L}{4} \le x \le \frac{3L}{4} \\ 0.3553209292\sin(2.064358612x) + 0.9443709067\cos(2.064358612x) \\ +2.182000163sinh(2.064358612x) - 2.146432446cosh(2.064358612x), & \frac{3L}{4} \le x \le L \end{cases}$$

$$Y(x)_{Second\ mode} = \begin{cases} \sin(2.460571808x) - 0.1205208154\cos(2.460571808x) \\ -0.5110834174sinh(2.460571808x) - 0.1205208154cosh(2.460571808x), & 0 \le x \le \frac{L}{4} \\ -0.2770052903\sin(2.460571808x) + 0.7818133785\cos(2.460571808x) \\ +1.357837437sinh(2.460571808x) - 1.144198329cosh(2.460571808x), & \frac{L}{4} \le x \le \frac{3L}{4} \\ -0.7010521306\sin(2.460571808x) - 0.7232227623\cos(2.460571808x) \\ -3.715192781sinh(2.460571808x) + 3.681844159cosh(2.460571808x), & \frac{3L}{4} \le x \le L \end{cases}$$

$$Y(x)_{Third\ mode} = \begin{cases} \sin(7.876011195x) - 0.03074534299\cos(7.876011195x) \\ -0.2338887417sinh(7.876011195x) - 0.03074534299cosh(7.876011195x), & 0 \le x \le \frac{L}{4} \\ 1.721252241\sin(7.876011195x) + 1.683743245\cos(7.876011195x) \\ +6.558092451sinh(7.876011195x) - 6.563075140cosh(7.876011195x), & \frac{L}{4} \le x \le \frac{3L}{4} \\ -0.008703728147\sin(7.876011195x) + 1.000417544\cos(7.876011195x) \\ +348.4367989sinh(7.876011195x) - 348.4367217cosh(7.876011195x), & \frac{3L}{4} \le x \le L \end{cases}$$

The first three transverse vibration bending mode shapes are shown in **Fig. 2**.

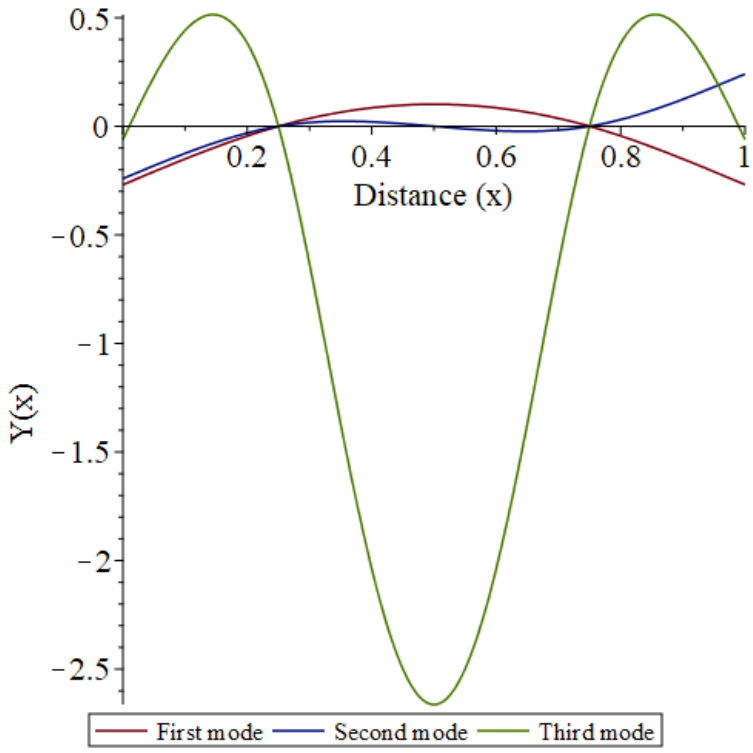

Fig. 2: *First three mode shapes obtained analytically*

3. Model validation using FEA

The beam's geometry was modelled as a prismatic member with an overall length of 1000 mm and a uniform square cross-section of 5 mm × 5 mm. A centrally supported span with symmetric overhangs on both sides was the outcome of imposing boundary conditions by placing fixed supports 250 mm from each end of the beam. In order to faithfully capture the intended structural restrictions in the numerical model, this configuration was chosen.

A structured meshing technique was used for discretisation to preserve numerical stability and homogeneity across the domain. There were 200,000 elements in all, with a constant element size of 0.5 mm employed across the length and cross-section. Standard mesh metrics were used to evaluate the mesh's quality. The skewness value, measured at 1.328×10^{-10}, was incredibly low, and the aspect ratio of the elements was zero, suggesting no elemental distortion. The elements' good shape and the minimal numerical errors caused by the mesh quality are confirmed by such a low skewness. The analysis was performed using a modal analysis setup configured to extract the first three bending vibration mode shapes.

The problem, when solved to find the first three mode shapes, yielded results as shown in **Fig. 3, Fig. 4,** and **Fig. 5**.

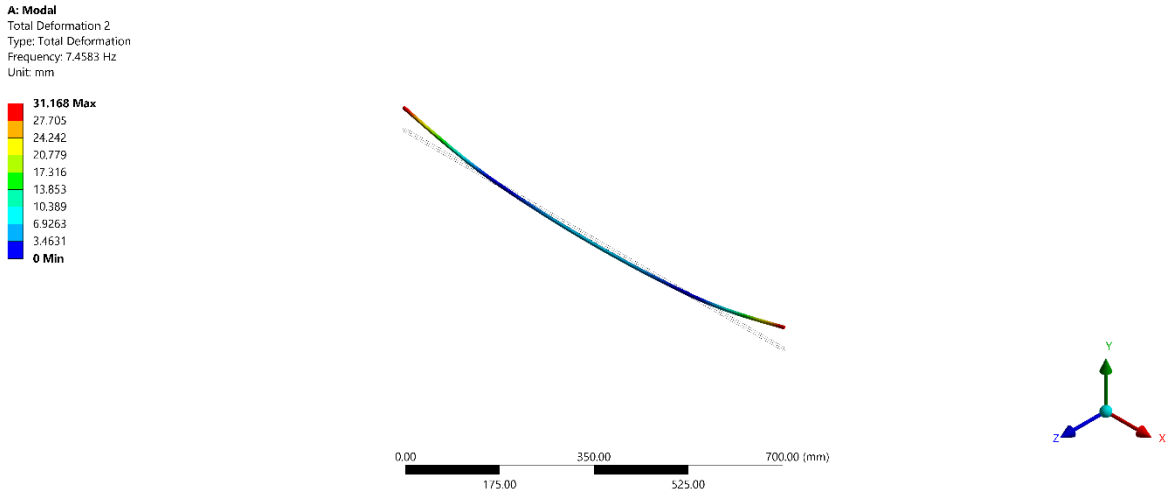

Fig. 3: First mode shape obtained from simulation

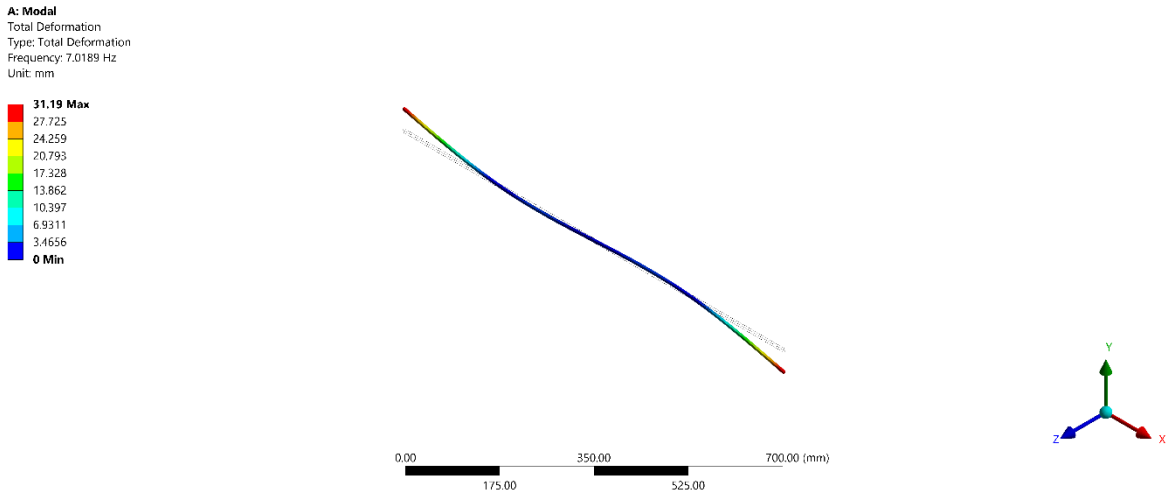

Fig. 4: Second mode shape obtained from simulation

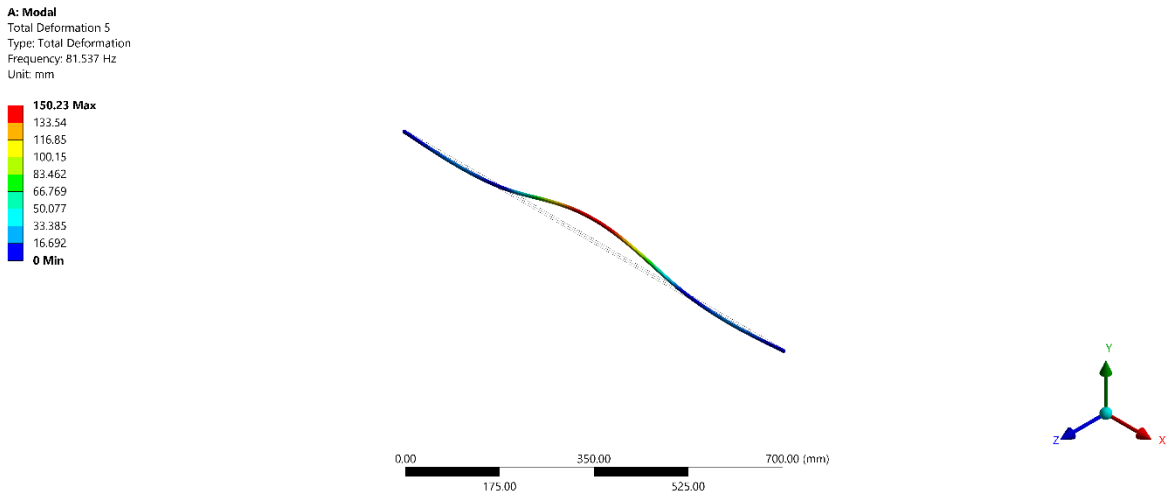

Fig. 5: Third mode shape obtained from simulation

4. Results and Discussion

From the analytical formulation, the first three bending natural frequencies are obtained as 4.9396 Hz, 7.016 Hz, and 71.9266 Hz, whereas the corresponding values from the simulation model are 7.4583 Hz, 7.0189 Hz, and 81.537 Hz. The differences arise due to the contrasting assumptions in the two approaches. The analytical solution assumes an ideal Euler–Bernoulli beam with continuous system representation and simplified boundary conditions, neglecting shear deformation, rotary inertia, and local stiffness or mass variations. In contrast, the simulation model uses finite discretization, applies boundary conditions at nodal points rather than exact mathematical locations, and includes a more realistic distribution of mass and stiffness, along with solver-related effects that may slightly shift the frequencies.

The mode forms derived from the analytical and simulation models show very close agreement in terms of deformation patterns and nodal locations, despite the observed variations in the natural frequencies. All of the simulation's bending modes, including the node and antinode locations and curvature, closely match the expected shape that was predicted theoretically. Despite some frequency shifts brought on by discretization, boundary condition approximation, and the addition of shear and rotating inertia effects, this strong correlation shows that the simulation faithfully depicts the dynamic behavior of the beam. The mode shape agreement offers compelling proof that the simulation accurately captures the structure's vibrational properties, guaranteeing the validity and dependability of the numerical results for additional research or design.

5. Conclusion

For the vibration analysis of a pinned–pinned double-overhung beam with lumped masses at its free ends, a transcendental mode shape formulation has been presented in this study. There is a close agreement for the higher modes, while the first mode shows a relatively larger difference because of its sensitivity to modelling assumptions. Analytical predictions of the bending frequencies show deviations of about 50.9%, 0.04%, and 13.4% from the corresponding finite element results for the first three modes, respectively. In spite of this, the curvature and nodal locations of the mode shapes obtained from the two methods show good consistency. These verify that the suggested theoretical framework offers a solid and quantitative foundation for forecasting the bending frequencies and mode shapes of double-overhung beams, making it an invaluable instrument for beam dynamics numerical research.

Conflicts of Interest

The authors confirm that there are no financial conflicts of interest or personal relationships that might have affected the findings of this study.

References

Alzghoul, M., Cabezas, S., & Szilágyi, A. (2022). Dynamic modeling of a simply supported beam with an overhang mass. *Pollack Periodica*, *17*(2), 42–47. https://doi.org/10.1556/606.2022.00523

Banerjee, J. R. (2012). Free vibration of beams carrying spring-mass systems − A dynamic stiffness approach. *Computers & Structures, 104–105,* 21–26. https://doi.org/10.1016/j.compstruc.2012.02.020

Civalek, Ö., & Ülker, M. (2004). Free Vibration Analysis of Elastic Beams Using Harmonic Differential Quadrature (HDQ). *Mathematical and Computational Applications, 9*(2), 257–264. https://doi.org/10.3390/mca9020257

Luintel, M. C. (2023). *Textbook of Mechanical Vibrations*. Springer Nature Singapore.

Rao, S. S. (2017). *Mechanical Vibrations*. Pearson Education, Incorporated.

Wang, Z., Hong, M., Xu, J., & Cui, H. (2014). Analytical and experimental study of free vibration of beams carrying multiple masses and springs. *Journal of Marine Science and Application*, *13*(1), 32–40. https://doi.org/10.1007/s11804-014-1231-4

Wu, J.-S., & Chen, D.-W. (2003). Bending vibrations of wedge beams with any number of point masses. *Journal of Sound and Vibration*, *262*(5), 1073–1090. https://doi.org/10.1016/S0022-460X(02)01084-2